Optical Receiver for Coherently Detected Pulse-Position Modulated Signals in the Presence of Atmospheric Turbulence

M. Muñoz Fernández[1,2] and V. A. Vilnrotter[2]

Performance analysis and experimental verification of a coherent free-space optical communications receiver in the presence of simulated atmospheric turbulence is presented. Bit-error rate (BER) performance of ideal coherent detection is analyzed in Section II, and the laboratory equipment and experimental setup used to carry out these experiments are described. The key components include two lasers operating at a 1064-nm wavelength for use with coherent detection, a 16-element (4×4) focal-plane detector array, and a data acquisition and signal processing assembly needed to sample and collect the data and analyze the results. The detected signals are combined using the least-mean-square (LMS) algorithm. In Section III, convergence of the algorithm for experimentally obtained signal tones in the presence of atmospheric turbulence is demonstrated.

In Section IV, adaptive combining of experimentally obtained heterodyned pulse-position modulated (PPM) signals with pulse-to-pulse coherence, in the presence of simulated spatial distortions resembling atmospheric turbulence, is demonstrated. The adaptively combined PPM signals are phased up via an LMS algorithm suitably optimized to operate with PPM in the presence of additive shot noise. A convergence analysis of the algorithm is presented, and results with both computer-simulated and experimentally obtained PPM signals are analyzed.

I. Introduction

Optical space communications systems are becoming more practical as technology develops, and they offer significant advantages over radio frequency (RF) communications. The main advantages are the ability to concentrate power in extremely narrow beams, the potential increase in modulation bandwidth, and the drastic reduction in component sizes. Optical wavelengths are very short and correspond to very high carrier frequencies. Increasing the carrier frequency theoretically increases the available transmission

[1] Graduate student, Electrical Engineering, California Institute of Technology.

[2] Communications Architectures and Research Section.

The research described in this publication was carried out by the Jet Propulsion Laboratory, California Institute of Technology, under a contract with the National Aeronautics and Space Administration.

bandwidth and, therefore, the information capacity of the system. As a result, frequencies in the optical range may have potential bandwidths of approximately 10^5 times that of a carrier in the RF range [1].

Laser communications performance is affected by the atmosphere because it is a dynamic and imperfect medium. Atmospheric channel effects include fluctuations in the signal amplitude, phase, and attenuation. However, space- and ground-based optical communications offer potential advantages in bandwidth over traditional RF communications and conventional microwave technology. Small beam divergence, small size, and large information bandwidth due to operation at a higher frequency are all advantages of a laser system. Transmitters and receivers are smaller and lighter for a specified distance; a laser requires lower power for a given distance; and lasers provide higher security and greater resistance to interference.

The use of a laser beam as a carrier for a satellite-to-ground link enables transmission using very narrow beam-divergence angles. Inhomogeneity in the temperature and pressure of the atmosphere leads to variations of the refractive index and the transmission path. Since the index of refraction of air is not uniform, it distorts the electromagnetic wave passing through it. Therefore, a laser beam traversing the atmosphere is constantly being refracted, or bent, and as a result scintillation occurs [1]. This turbulence-induced fading impairs free-space optical links in much the same way that flat multipath fading impairs radio-frequency wireless links. These variations of refracted index as well as pointing vibrations can cause fluctuations in the intensity and phase of the received signal, leading to an increase in link-error probability.

Absorption by water vapor reduces the energy content in the communication beam, and turbulence increases the beam's divergence. The three main atmospheric processes that affect optical wave propagation are absorption, scattering, and refractive-index fluctuations. Index of refraction fluctuations lead to irradiance fluctuations, beam broadening, and loss of spatial coherence of the optical wave at the receiver. In the context of optical communications, this randomization of the optical phase front often requires the use of a larger receiver field of view, thus admitting more unwanted background radiation into the receiver. In the presence of background radiation, the performance of direct-detection optical receivers often degrades significantly. One way to overcome the effects of background radiation is to use coherent detection, which is generally much less sensitive to background effects than is direct detection [2]. In addition, detectors used for coherent detection have higher quantum efficiency than those used for direct-detection photon-counting applications. The solution proposed here is to use focal-plane arrays to collect optical signals from different spatial modes of the received signal field simultaneously, and then to recombine the signals optimally. Analysis and a proof-of-concept demonstration of coherent adaptive array detection with pulse-position modulated (PPM) signals will be described in the following sections.

With coherent detection, the local oscillator mixes with the modulated wave at the surface of the photodetector, as shown in Fig. 1 [3]. The coherent detector converts phase changes in the optical carrier to phase changes in the optical intensity, which are reproduced in the detected current waveform.

Optical receivers can be divided into two basic types [1]: (1) power-detecting, direct-detection or noncoherent receivers and (2) heterodyning or coherent receivers. The simplest implementation is achieved with direct detection, where the lens system and photodetector operate to detect the instantaneous power in the collected field as it arrives at the receiver. Intensity modulation with direct detection is currently used for optical communications systems. Under ideal transmission and detection conditions, the probability of detecting n photons in a pulse train having an average of K_S detected photons per pulse obeys the Poisson distribution [1,2]

$$p(n) = \frac{K_S^n e^{-K_S}}{n!} \tag{1}$$

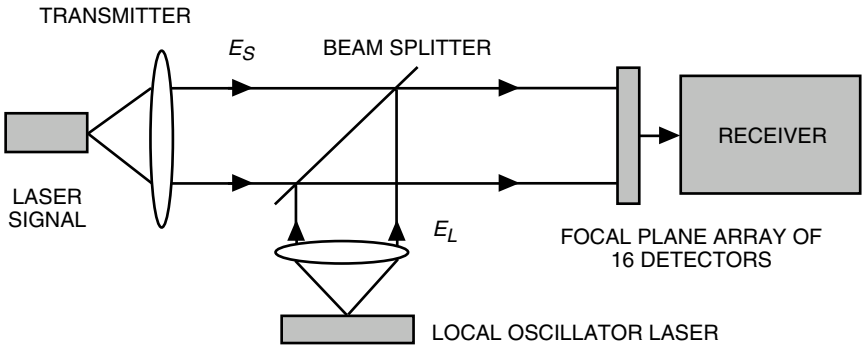

Fig. 1. Configuration of the coherent optical receiver.

The probability of an erasure is defined as the detection of no photons during the pulse and is given by

$$P_E = \exp(-K_S) \tag{2}$$

An average of 21 detected photons per pulse would be needed to achieve an erasure probability of 10^{-9}. This erasure probability is rarely reached since it assumes no dark or background counts whatsoever in the receiver. In the presence of background radiation, performance of direct-detection receivers degrades significantly, as shown in [1]. One way to overcome the effects of background radiation is to use coherent detection. With coherent detection, the local oscillator (LO) mixes with the modulated wave at the photodetector. If the LO field amplitude (E_L) is at the same wavelength as the received optical signal field amplitude, (E_S), and in addition is in phase with the optical carrier, the detection is called homodyne detection. If the frequencies of the LO and received signal are different, then it is called heterodyne detection. The heterodyne detector converts phase changes in the optical carrier to phase changes in the optical intensity, which are reproduced in the detected current waveform. The following analysis shows how the heterodyne scheme permits detection of the incoming signal beam. If the incident beams are perfectly parallel plane waves and have precisely the same polarization, the total field is the sum of the two constituent fields. Taking the squared magnitude of the sum of the complex amplitudes, the expression for the intensity on the photodetector surface is [5,6]

$$\begin{aligned} I &\propto \left| E_S \exp\left(j\omega_S t + \phi_S\right) + E_L \exp\left(j\omega_L t + \phi_L\right)\right|^2 \\ &= E_S^2 + E_L^2 + 2E_S E_L \cos\left[\left(\omega_S - \omega_L\right) t + \left(\phi_S - \phi_L\right)\right] \end{aligned} \tag{3}$$

where E_S and E_L are real magnitudes of the signal and local fields, respectively, ω_S is the signal frequency, ϕ_S is the signal phase, and ω_L and ϕ_L are the frequency and phase, respectively, of the LO.

This inherent squaring operation at the photodetector produces a detector current at the intermediate frequency (IF) which contains the signal modulation. High-frequency intensity components that oscillate at twice the optical carrier frequency have been eliminated from the receiver because that frequency is much greater than the frequency response of the detector [4]. The detected current is proportional to the average optical intensity, where the average is taken over a time interval that is long compared to the optical period, but short compared to the period of the IF.

If the local oscillator power is much greater than the signal power, the second term of Eq. (3) can be neglected. The first term represents a large and continuous signal that carries no information but generates a shot-noise contribution. The third term represents the signal modulation. If the signal is AC-coupled to eliminate the local oscillator signal, then

$$i(t) \propto 2E_S E_L \cos\left[(\omega_S - \omega_L)t + \phi_S - \phi_L)\right] \tag{4}$$

In coherent communications, the optical frequency and the phase of the signal relative to the local oscillator are preserved. Shot-noise-limited SNR obtained in homodyne detection is a factor of two (3-dB) greater than that of a heterodyne receiver and a factor of four (6-dB) better than the SNR of a direct-detection system [6]. With heterodyne and homodyne optical detection, quantum-limited performance theoretically can be obtained, and receiver sensitivities on the order of 10- to 20-dB higher than direct-detection systems are possible under high background conditions [7].

II. Performance Analysis of a Coherent Optical Receiver for *M*-ary PPM Signals

When coherent detection is used, digital bits can be encoded directly on the phase or frequency of the laser carrier itself. The received modulated laser carrier can be translated to a lower RF frequency, where the digital modulation can be decoded using standard decoding techniques [1]. In the heterodyne detection system examined, pulse-position modulation (PPM) is used. PPM is a form of block encoding in which bits are transmitted in blocks instead of one at a time [1]. Optical block encoding is achieved by converting each block of k bits into one of $M = 2^k$ optical fields of transmission. At the receiver end, decoding of each block is performed by determining which one of the M fields is received per block time. For the PPM case, a PPM frame contains M slots, and an optical pulse is placed in one of those M slots. The data word is determined based on the position of the optical pulse in the frame. The receiver decides on the basis of maximum-likelihood symbol detection; it selects the slot with the greatest energy, and the symbol that contains a signal pulse in that slot location is declared to be the transmitted symbol.

If A is the aperture of the detector, $\alpha = \eta_q/h\nu$, where η_q is the detector quantum efficiency, h is Planck's constant, and $\nu = \omega/2\pi$ is the optical frequency, and $E_L \gg E_S$, from Eq. (3) and [1] the resulting intensity counting rate process of the photodetector is $\alpha A E_L^2 + \alpha A 2E_S E_L \cos\left[(\omega_S - \omega_L)t + \phi_S - \phi_L)\right]$. We assume that local power alone sets the shot noise level of spectral level $N_S/2$.

Under shot-noise-limited conditions, and after filtering out the DC term, the detector can be modeled as

$$r(t) = s(t) + n(t) \tag{5}$$

where $n(t)$ is a Gaussian noise process of spectral level $N_S/2 = \alpha A E_L^2$. The variance of the shot noise is calculated by integrating for τ seconds (the duration of the PPM pulse), resulting in $\sigma_S^2 = \alpha A E_L^2 \tau$ [1]. The value of the signal for homodyne detection is also obtained by integrating for τ seconds over the signal slot, resulting in $2E_S E_L \alpha A \tau$. For homodyne detection, $\omega_L = \omega_S$ and $\phi_L = \phi_S$. The signal-to-noise ratio therefore is

$$\text{SNR} = \frac{P_{\text{signal}}}{P_{\text{noise}}} = \frac{\left[2E_S E_L \alpha A \tau\right]^2}{\alpha A E_L^2 \tau} = 4\alpha A E_S^2 \tau = 4K_S \tag{6}$$

where $K_S = \alpha A E_S^2 \tau$ is the average number of signal photons over the slot duration. For the case of heterodyne detection, the frequencies are not equal ($\omega_L \neq \omega_S$) and the signal becomes

$$s(t) = 2\alpha A E_S E_L \cos\left[(\omega_S - \omega_L)t\right] \tag{7}$$

with rms value $(2/\sqrt{2})E_S E_L \alpha A \tau = \sqrt{2} E_S E_L \alpha A \tau$. Following the derivation in [9] and applying Campbell's theorem, this results in the signal-to-noise ratio for heterodyne detection:

$$\text{SNR} = \frac{\left[\sqrt{2} E_S E_L \alpha A \tau\right]^2}{\alpha A E_L^2 \tau} = 2\alpha A E_S^2 \tau = 2K_S \tag{8}$$

The strong local field generates a high count rate at the detector output, which gives rise to Gaussian shot noise. Therefore, heterodyne detector outputs are assumed to be Gaussian processes with the signal term corresponding to the modulated carrier, and shot-noise components are considered as additive Gaussian noise with the spectral level given above. As a result, the photo-detected field can be modeled as a Gaussian process, with mean $2E_S E_L \alpha A \tau$ for homodyne detection and $\sqrt{2} E_S E_L \alpha A \tau$ for heterodyne detection, and the variance in both cases is $\sigma_S^2 = \alpha A E_L^2 \tau$. The probability density therefore can be written as $p(x) = (1/\sqrt{2\pi\sigma^2}) e^{-(x-\eta)^2/2\sigma^2}$, where η is a mean value due to the signal energy.

The probability of correct PPM detection is the probability that one Gaussian random variable with mean η (corresponding to the signal slot) exceeds $(M-1)$ other zero-mean Gaussian random variables (corresponding to the noise slots). Therefore, the probability of correct symbol detection for the signal slot can be viewed as a Gaussian random variable with mean equal to the corresponding SNR and unit noise variance

$$p_{\text{SIGNAL SLOT}}(x) = \frac{1}{\sqrt{2\pi}} e^{-\left(x - \sqrt{\text{SNR}}\right)^2/2} \tag{9}$$

with $\text{SNR} = 4K_S$ for homodyne detection and $\text{SNR} = 2K_S$ for heterodyne detection. For the remaining slots with no signal, the process could be modeled as a Gaussian random variable with zero mean and unit variance

$$p_{\text{NOISE SLOT}}(x) = \frac{1}{\sqrt{2\pi}} e^{-x^2/2} \tag{10}$$

Because PPM signals are a type of orthogonal signals, for the homodyne detection case the probability of correct symbol detection $P(SC)$ can be expressed as [9,10]

$$P(SC) = \int_{-\infty}^{+\infty} \frac{1}{\sqrt{2\pi(\alpha E_L^2 A\tau)}} e^{(x - 2\alpha E_S E_L A\tau)^2/2(\alpha_L^2 A\tau)} dx \left[\int_{-\infty}^{x} \frac{1}{\sqrt{2\pi(\alpha E_L^2 A\tau)}} e^{-y^2/2(\alpha E_L^2 A\tau)} dy\right]^{m-1} \tag{11}$$

where $\eta = 2\alpha E_S E_L A\tau$.

With the change of variables $z = y/\sqrt{\alpha E_L^2 A\tau}$ and $dz = dy/\sqrt{\alpha E_L^2 A\tau}$, and noting that, when $y = x$, $z = x/\sqrt{\alpha E_L^2 A\tau}$, the following simplified equation is obtained:

$$P(SC) = \int_{-\infty}^{+\infty} \frac{1}{\sqrt{2\pi(\alpha E_L^2 A\tau)}} e^{(x-2\alpha E_S E_L A\tau)^2/2(\alpha E_L^2 A\tau)} dx \left[\int_{-\infty}^{x/\sqrt{\alpha E_L^2 A\tau}} \frac{1}{\sqrt{2\pi}} e^{-z^2/2} dz \right]^{M-1} \tag{12}$$

Then with another change of variables, $w = x/\sqrt{\alpha E_L^2 A\tau}$ and $dw = dx/\sqrt{\alpha E_L^2 A\tau}$, we get

$$\begin{aligned} P(SC) &= \int_{-\infty}^{+\infty} \frac{1}{\sqrt{2\pi}} e^{-[(w-\sqrt{4\alpha E_S^2 A\tau})^2/2]} dw \left[\int_{-\infty}^{w} \frac{1}{\sqrt{2\pi}} e^{-(z^2/2)} dz \right]^{M-1} \\ &= \int_{-\infty}^{+\infty} \frac{1}{\sqrt{2\pi}} e^{-[(w-\sqrt{4K_S})^2/2]} dw \left[\int_{-\infty}^{w} \frac{1}{\sqrt{2\pi}} e^{-(z^2/2)} dz \right]^{M-1} \end{aligned} \tag{13}$$

or

$$P(SC) = \int_{-\infty}^{+\infty} \frac{1}{\sqrt{2\pi}} e^{-[(w-\sqrt{4K_S})^2/2]} dw \big[1 - Q(w)\big]^{M-1} \tag{14}$$

where $Q(w) = \int_x^{\infty} (1/\sqrt{2}\pi) e^{-z^2/2} dz$

Similarly, the probability of symbol detection for the heterodyne case becomes

$$P(SC) = \int_{-\infty}^{+\infty} \frac{1}{\sqrt{2\pi}} e^{-[(w-\sqrt{2K_S})^2/2]} dw \big[1 - Q(w)\big]^{M-1} \tag{15}$$

These expressions are accurate under strong local field conditions and negligible background radiation. If equal a priori transmission probabilities are assumed for each symbol, the probability of symbol error [1] can be expressed as

$$P(SE) = 1 - P(SC) \tag{16}$$

The bit-error probability P_e is related to the probability of symbol error through

$$P_e = \left[\frac{M/2}{M-1} \right] P(SE) \tag{17}$$

Finally, the bit-error probability for homodyne detection is given by

$$\begin{aligned} P_e &= \frac{M/2}{M-1} \left[1 - \left\{ \int_{-\infty}^{+\infty} \frac{1}{\sqrt{2\pi}} e^{-(w-\sqrt{4K_s})^2/2} dw \big[1 - Q(w)\big]^{M-1} \right\} \right] \\ &= \frac{M/2}{M-1} \left[1 - \left\{ \int_{-\infty}^{+\infty} \frac{1}{\sqrt{2\pi}} e^{-(w-\sqrt{4K_s})^2/2} dw \left[\frac{1}{2} - \frac{1}{2} erf\left(\frac{w}{\sqrt{2}} \right) \right]^{M-1} \right\} \right] \end{aligned} \tag{18}$$

For heterodyne detection, the bit-error probability can be expressed as

$$P_e = \frac{M/2}{M-1}\left[1 - \left\{\int_{-\infty}^{+\infty} \frac{1}{\sqrt{2\pi}} e^{-(w-\sqrt{2K_s})^2/2} dw \left[\frac{1}{2} - \frac{1}{2} erf\left(\frac{w}{\sqrt{2}}\right)\right]^{M-1}\right\}\right] \tag{19}$$

A simple bound often applied in block detection analysis is the union bound. The probability of a finite union of events is bounded above by the sum of the probabilities of the constituent events. Since the binary test between any two decoding symbols is equivalent to an orthogonal coherent test, Eqs. (20) and (21) are obtained.

Following [9], the union bound for the case of homodyne detection is

$$P_e \cong \left(\frac{M}{2}\right) Q\left[\sqrt{2K_S}\right] = \left(\frac{M}{2}\right)\left\{\frac{1}{2} erfc\left[\sqrt{K_S}\right]\right\} \tag{20}$$

Similarly, the union bound for the bit-error probability for heterodyne detection becomes

$$P_e \cong \left(\frac{M}{2}\right) Q\left[\sqrt{K_S}\right] = \left(\frac{M}{2}\right)\left\{\frac{1}{2} erf\left[\frac{\sqrt{K_s}}{2}\right]\right\} \tag{21}$$

Figures 2 and 3 show the exact bit-error probabilities and union bound approximation for optical heterodyne and homodyne detection of PPM signals with $M = 2, 4, 8, 16$ slots. Note that as M increases the bit-error probability is higher because we are plotting versus the average number of photons per pulse and not per bit.

III. Experiment Description

The experimental setup of the optical coherent combining experiment consists of two Nd:YAG lasers operating at 1064 nm, whose outputs are aligned and combined on the surface of a 4×4 detector array. One of the lasers serves as a local oscillator while the other simulates the received signal. Due to large relaxation oscillation below 1 MHz, the current setup is a heterodyne detection receiver where the two lasers are operated at slightly different wavelengths, yielding a relatively stable difference-frequency tone of

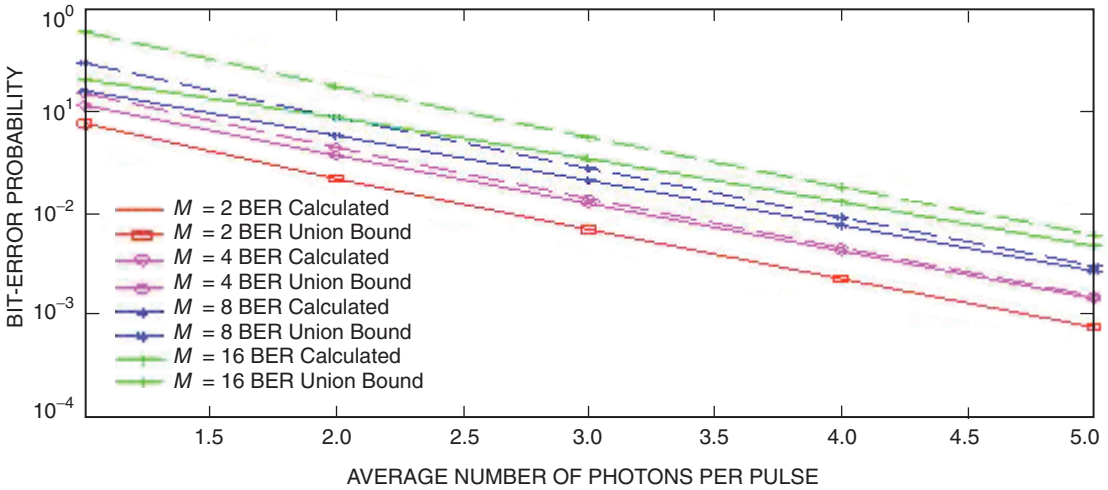

Fig. 2. BER for optical homodyne detection.

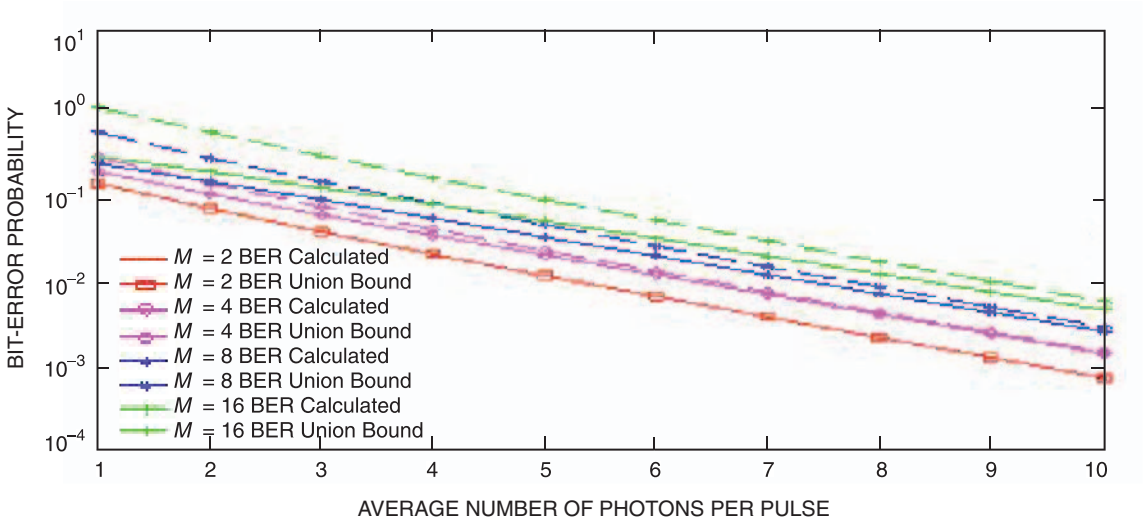

Fig. 3. BER for optical heterodyne detection.

approximately 6 MHz in the detected signal. The difference-frequency tone is generally observed in several array elements simultaneously, but usually with different phases. If the detector element outputs were simply summed, the addition of out-of-phase signal components could result in significant cancellation, yielding a weak signal tone at the output. However, if individual detector elements over which the signal field is essentially coherent are processed separately, then the outputs can be phase aligned prior to addition, effectively recovering the lost signal power.

Figure 4 is a photograph of the optical setup. In the current coherent combining experiment, each of the 16 outputs of the detector array is amplified and input to a 16-channel data-acquisition assembly. The analog signals are digitized to 8 bits at a sampling rate of 25 mega-samples per second (MSPS). The data-acquisition system is capable of synchronously recording up to 1 megabyte of data per channel. Five channels that contained significant signal energy were identified, and samples from each channel were collected synchronously. The modulation beat notes can be observed (Fig. 7) at a rate of approximately 100 kHz, resulting in a PPM frame period of approximately 10 μs, only half of which is used for information with this modulator. Since the slot width is 300 ns, there are approximately 16 disjoint pulse widths in a half-frame, yielding approximately a 16-PPM communications system with dead time (this modulator was originally used for Q-switched laser applications, where including a dead time was appropriate). Note, however, that if the entire frame were used, as would be the case in a realistic communications application, then the entire frame could carry information, resulting in a 32-PPM communications system.

A snapshot of an individual laser pulse that contains the coherently detected PPM beat note is shown in Fig. 5. The optical local oscillator frequency was displaced from the received optical signal frequency by 6 MHz, resulting in an intermediate detected frequency of 6 MHz. The heterodyned PPM intermediate signal was sampled at 25 MHz (40-ns samples), and the resulting sample stream digitally downconverted to complex baseband (this operation effectively upconverted the 488-kHz laser relaxation oscillation to 6.5 MHz), which was subsequently removed from the complex baseband samples by low-pass filtering. The resulting downconverted complex samples served as input to a least-mean-square (LMS) algorithm, which was used to estimate the complex weights required to reconstruct the signal. The complex-weighted samples from each channel were then combined in order to maximize the combined signal-to-noise ratio.

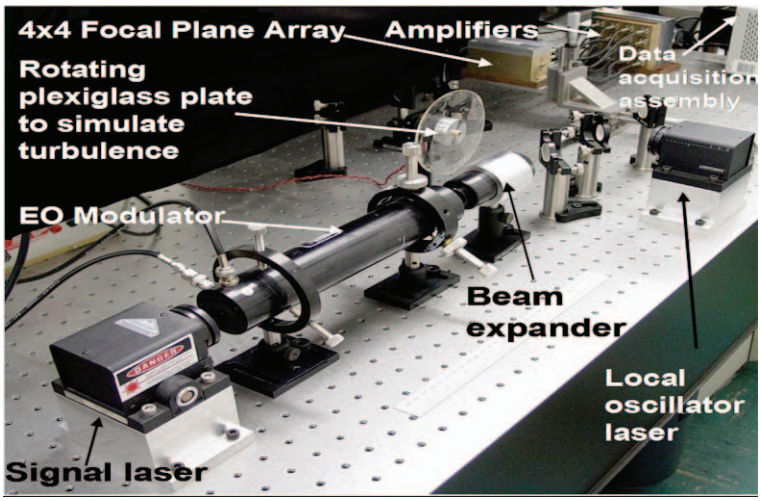

Fig. 4. Coherent combining experiment at the Jet Propulsion Laboratory (NASA).

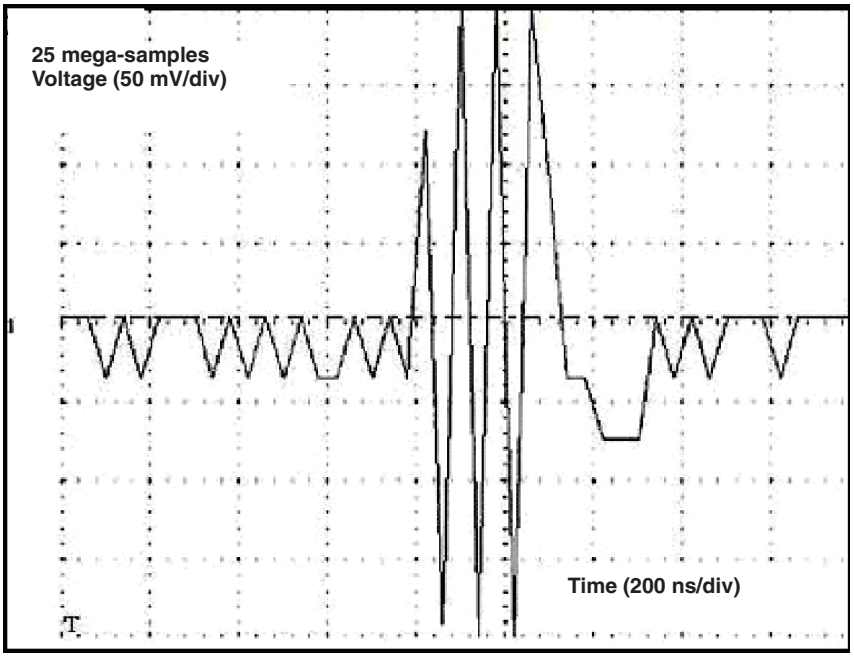

Fig. 5. Snapshot of an individual PPM pulse beat note.

A rotating pre-distorted plexiglass plate was incorporated into the experimental setup to simulate atmospheric turbulence. Intensity distributions of the signal beam at the input to the focal-plane array under ideal conditions and with simulated turbulence are shown in Figs. 6(a) and 6(b), respectively.

Figure 7(a) illustrates coherently detected PPM beat notes in four different channels under ideal conditions, and Fig. 7(b) shows them in the presence of atmospheric attenuation.

(a) (b)

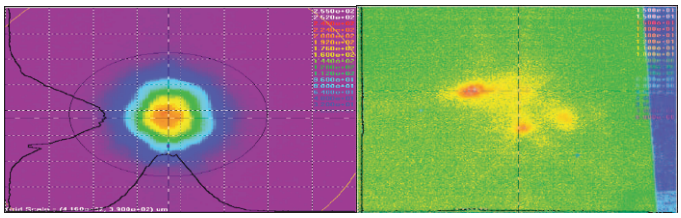

Fig. 6. Beam profile (a) under ideal (undistorted) conditions and (b) with simulated turbulence using a plexiglass plate.

(a)

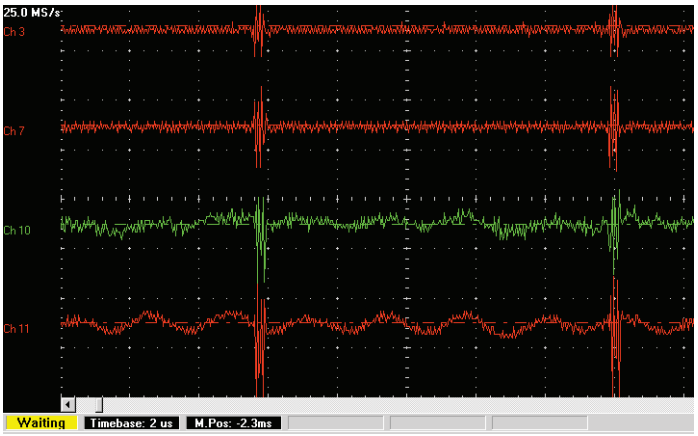

(b)

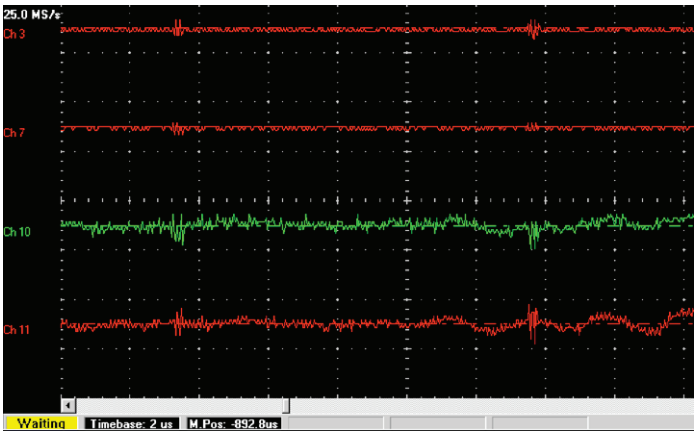

Fig. 7. Sampled sequences of 4 channels containing PPM-modulated 6-MHz beat notes (a) under ideal conditions and (b) in the presence of atmospheric turbulence.

IV. Adaptive Combining of Beat Notes Using the LMS Algorithm

The discrete complex version of the LMS algorithm can be described by the recursive equation [11,12]:

$$W_i(n+1) = W_i(n) + \mu S_i^*(n)\varepsilon(n) \tag{22}$$

The LMS is a recursive algorithm that allows the value of each weight, W_i, at the $(n+1)$ sample to be calculated from its value at the nth sample, using the signals at the nth sample. The sampled error signal is obtained from the sampled reference signal and array output, as follows:

$$\varepsilon(n) = d(n) - s(n) = d(n) - \sum_{i=1}^{N} W_i(n)S_i(n) \tag{23}$$

The LMS algorithm described in Eqs. (22) and (23) is complex in the sense that the input and output data as well as the weights are all complex values. In our experiments, the reference signal is a constant value, equal to the sum of the average magnitudes of the signals in the signal channels. The weights are computed from Eq. (22), starting with zero initial values. Varying the step size, it is possible to control the fraction of the current weight estimate applied during each update, providing a desired degree of smoothing to the weight estimates.

Small step size tends to produce good weight estimates under static conditions; however, it generally leads to greater weight misadjustment under dynamic conditions (such as severe Doppler or severe differential drift between local and signal wavelengths) as the weight estimates cannot keep up with the dynamics. Therefore, there is typically a best step size to use for each situation. After some experimentation, it was determined that for this data set good results could be obtained by correlating over 10,000 samples and using a step size of 1,000. After approximately 30 samples, the weights converge as maximum combined power and minimum error are obtained; that translates to 1.2 μs of acquisition time.

Previously obtained data have shown that for small values of step size ($\mu = 10$), the LMS algorithm cannot keep up with the phase variations in the beat note; plots of the combining output signal where the four channels are not perfectly combined showed that it oscillates and never reaches its maximum value of 0.06. The error signal never settled down to a small value. As the value of the step size was increased, with $\mu = 100$, performance was greatly improved. The combined output increased in value, approaching its maximum. The error signal decreased, showing partial convergence of the weights. Finally, when the step size is large enough so that the LMS algorithm is able to keep up with the phase rotation of the complex downconverted beat note, at $\mu = 1000$, as is shown in Fig. 8, the combined output signal reached its expected maximum value of 0.06.

With this optimum value of μ, the error approaches zero (Fig. 9), and it is concluded that the signals are phased up. Figure 10 shows the phase of the weights; the weights have a sawtooth shape, which is due to continuously changing phase in the downconverted output, which is not exactly at zero frequency, but very close to it.

Now the purpose is to analyze the case of a signal tone received in the presence of simulated atmospheric turbulence conditions using the rotating plexiglass plate shown in Fig. 4. Figure 6 represents the intensity distribution of the signal beam in the presence of simulated turbulence conditions.

The reference signal used in the algorithm for this situation resulted in a value of 0.0036 (Fig. 11). As in our previous case, four channels that contained significant signal were identified, and at a certain time 104,128 samples were synchronously collected from each channel. After some experimentation, it was determined that for this data set good results could be obtained by correlating over 10,000 samples

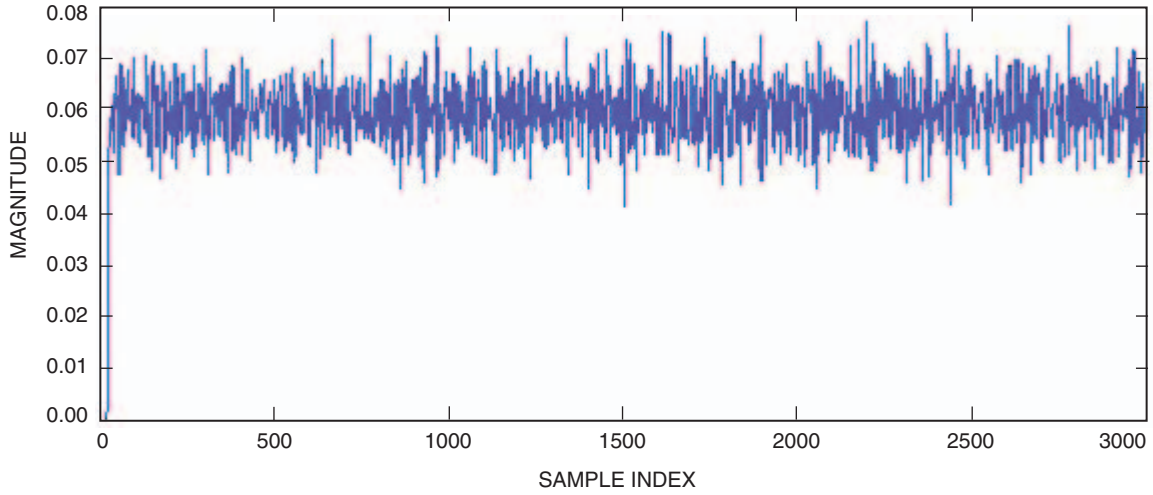

Fig. 8. Combined output power with μ = 1000.

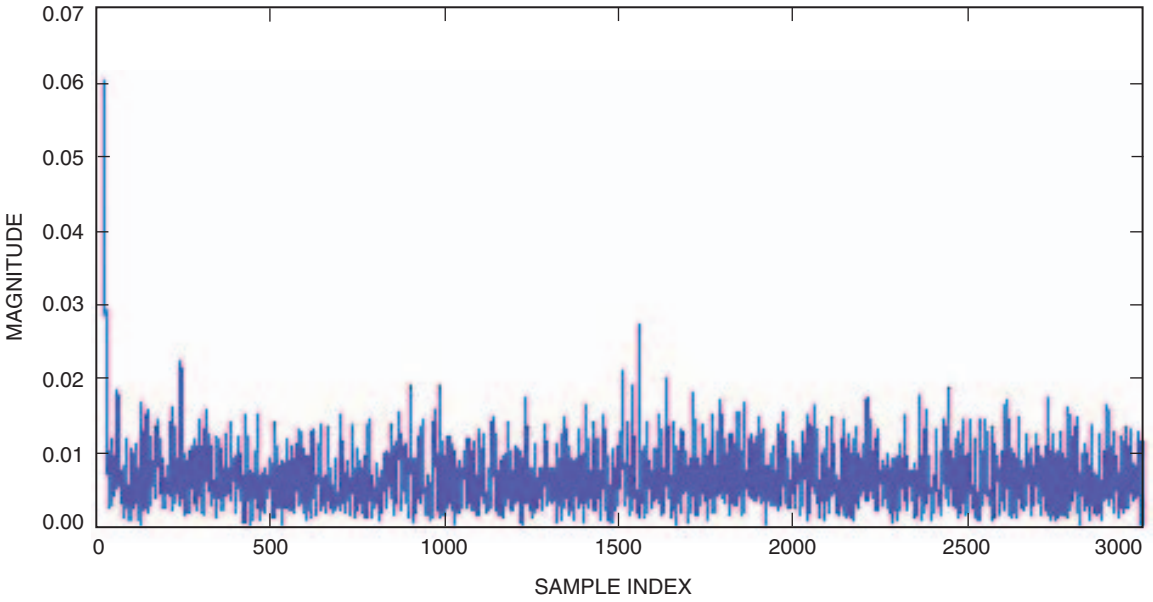

Fig. 9. Error signal with μ = 1000.

and using a step size of 20,000 because the signal is even weaker than for the ideal case due to the loss introduced by the atmospheric turbulence added to the system. Figure 11 shows the combined output that reaches its maximum value of 0.0036. Convergence of the LMS algorithm is accomplished after 200 samples, and therefore the acquisition time is 8 μs. In order to minimize higher-frequency noise contributions in this case, we use a narrower filter bandwidth on the signal processing block.

Figure 12 shows the phase of the weights with $\mu = 20,000$. For this case, the weights also have a sawtooth shape, due to continuously changing phase in the downconverted output because it is not exactly at 0 Hz.

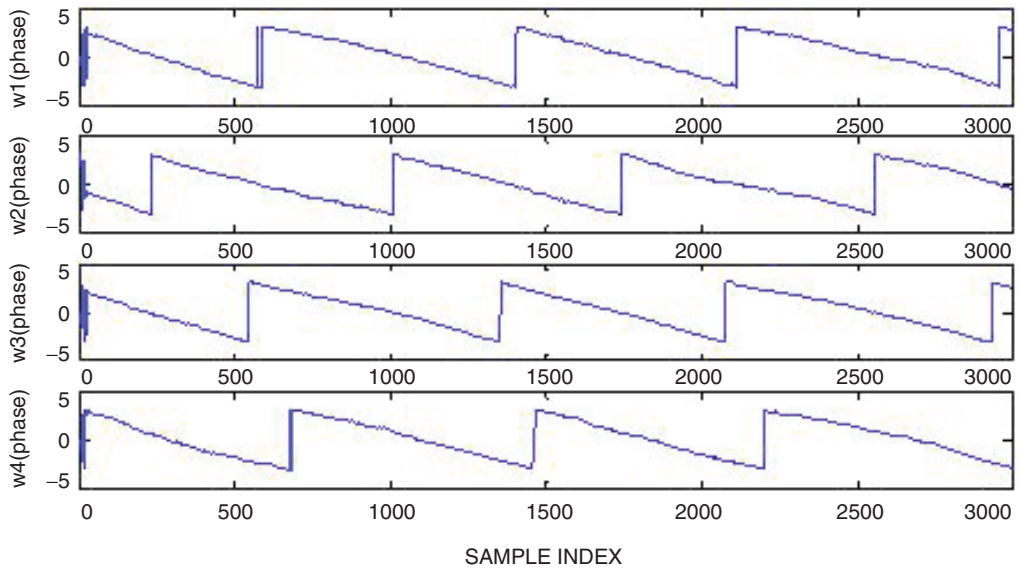

Fig. 10. Phase of the LMS weights for μ = 1000 **for four different channels.**

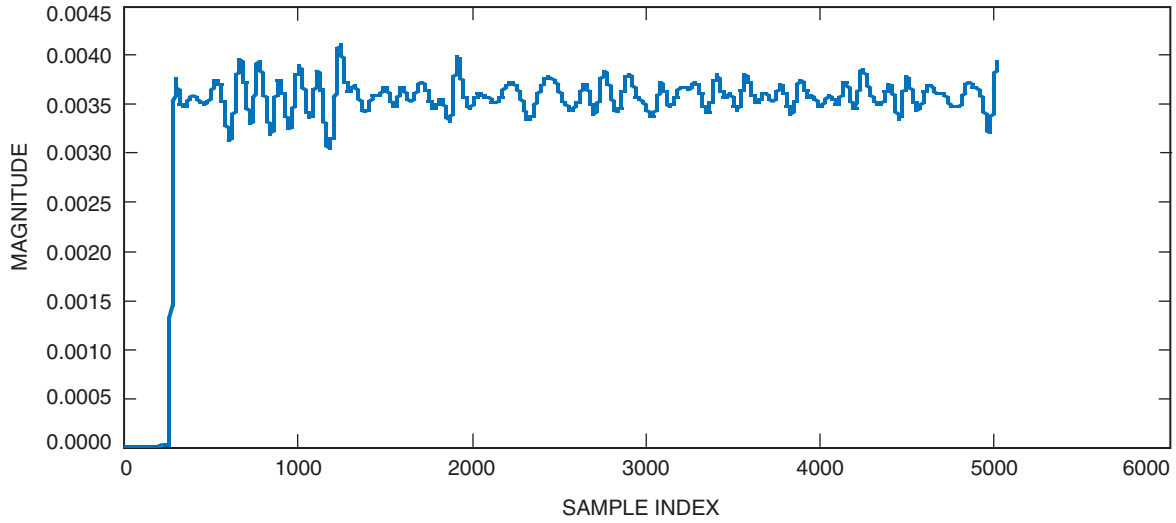

Fig. 11. Combined output power of the beat-note signal in the presence of simulated atmospheric turbulence with μ = 20,000.

Figure 13 shows the error signal that approaches zero when the step size is $\mu = 20,000$. Therefore, we have accomplished convergence of the LMS algorithm and obtained maximum combined output value with minimum error.

These results illustrate that increasing the step size allows the LMS algorithm to follow and track the phase rotation of the complex downconverted beat note in the presence of atmospheric turbulence conditions. It was found that a good value of μ for the particular case discussed here is 20,000 when there is accurate tracking of the signals, and accordingly the error signal approaches zero and maximum combined output is achieved. It is important to note that the step size in books and papers usually is shown to be much smaller than one, but that is because the signal is assumed to be of unity amplitude. In our experiment, the signal levels that we are dealing with are very small as there is not enough

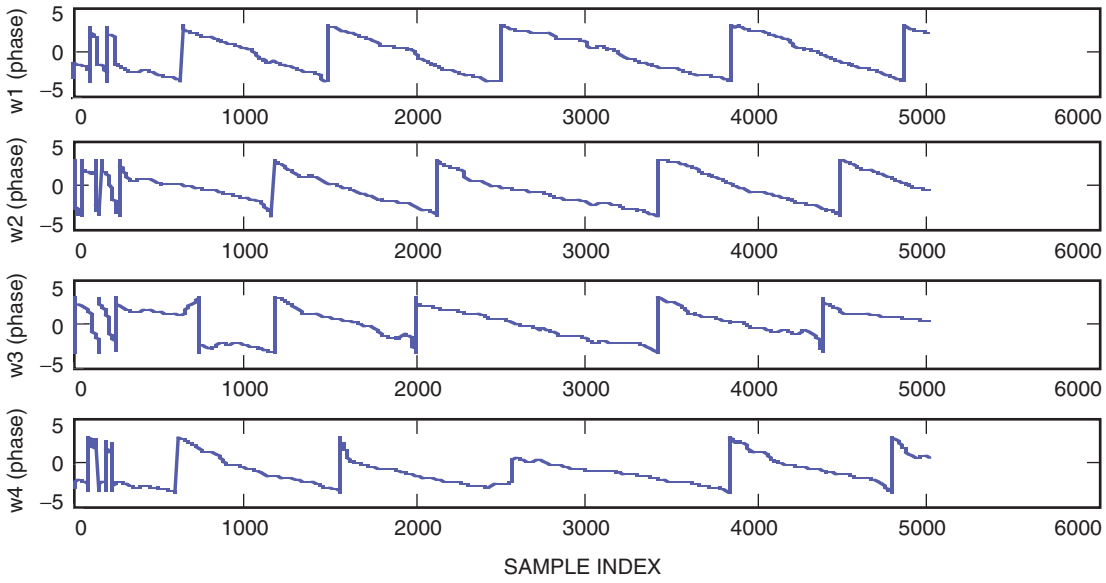

Fig. 12. Phase of the weights with μ = 20,000 for four different channels.

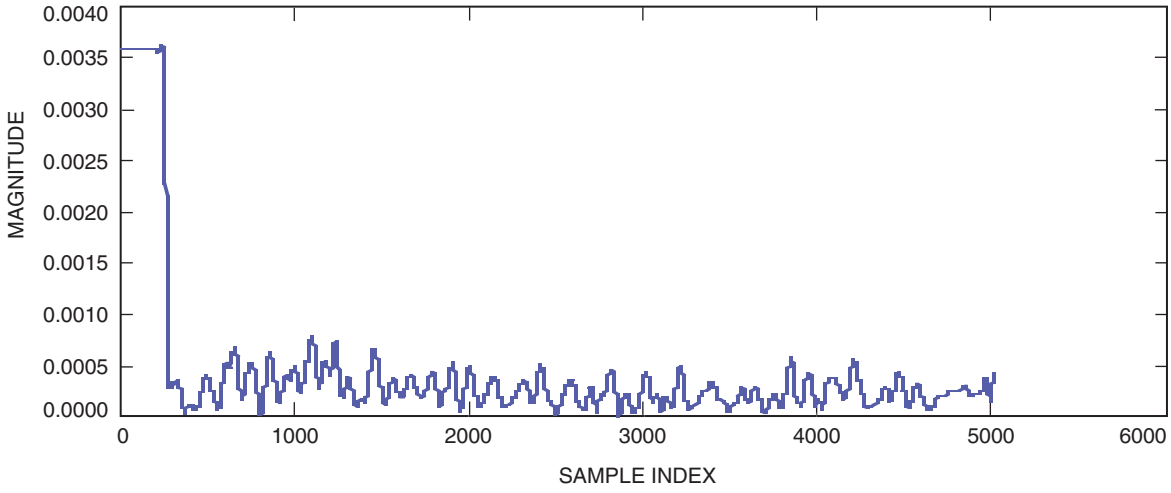

Fig. 13. Error signal with μ = 20,000.

amplification after detection. Therefore, large values of step size are needed to provide adequate updates to the weights.

A. Adaptive Combining of Simulated Data: Signal Tone and 32-PPM Signals

Convergence of the combining weights as a function of sample number has been analyzed (see the derivation in the Appendix). Several cases have been considered, including signal tone and PPM signal observed under ideal conditions. Figure 14 shows the comparison of the convergence of the LMS algorithm for the case of signal tone versus a 32-PPM signal. It has been demonstrated that the number of samples required to obtain convergence in the case of M-ary PPM signal with a peak power constraint is M times the number of samples required by a continuous tone, due to decreased total signal energy in the lower duty-cycle-modulated waveform. Therefore, for the simulated case of a signal tone, convergence is obtained after 4 samples, while for 32-PPM, 128 samples are required for convergence, as illustrated in Fig. 14 for $\mu = 1$ and an introduced phase weight variation of 1 radian between every channel.

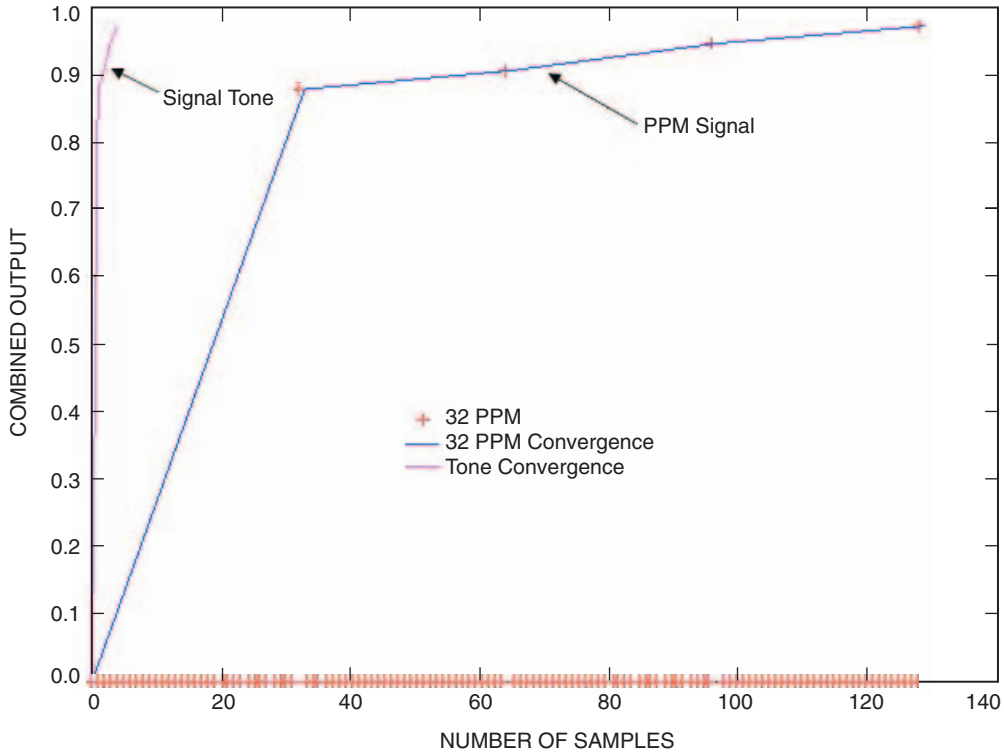

Fig. 14. Comparison of output convergence for signal tone and 32-PPM signal (real part of LMS output).

Figure 15 is a block diagram of the adaptive focal-plane array combining system, where there are N detectors and therefore there are N channels containing signals that undergo amplification, filtering, baseband downconversion, and adaptive combining with the LMS algorithm.

Figure 16 shows a comparison of convergence for a simulated signal tone and a simulated 32-PPM signal where the step size is $\mu = 0.003$ (detector array consists of 16 detectors). Convergence is obtained for a signal tone after 125 samples, and for the 32-PPM signal after 4000 samples, as expected. Increasing the step size to $\mu = 0.008$, the LMS algorithm converges faster; hence, only 1000 samples are needed for convergence as opposed to 4000 samples for the previous case.

B. Experimental Results

Small step size tends to produce accurate weight estimates under static conditions; however, the algorithm may not be able to keep up with rapid changes under dynamic conditions with a small step size. This often leads to weight misadjustment errors under dynamic conditions, as the weight estimates cannot keep up with the signal dynamics. Therefore, there is typically a best step size to use for each situation.

It is important to note that, in the literature, the step size is usually taken to be much smaller than one, but that is because the signal is assumed to be of unity amplitude. In our experiment, the signal levels tend to be very small as there is not enough amplification after detection. Therefore, larger values of step size are needed to provide adequate updates to the weights.

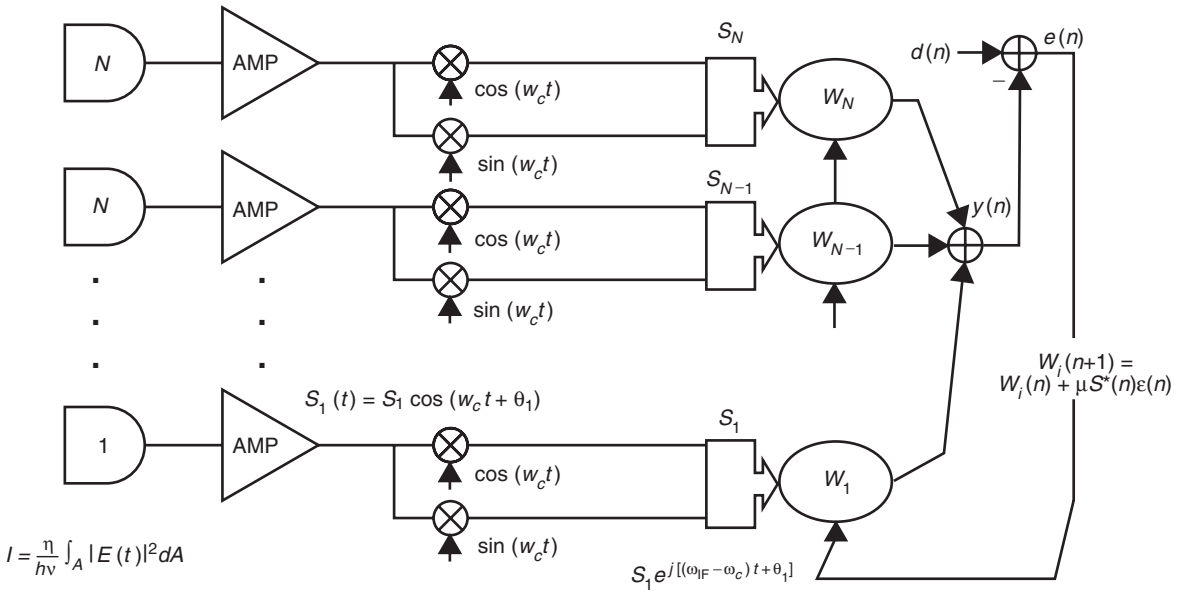

Fig. 15. System block diagram including signal-flow graph representation of the complex LMS algorithm.

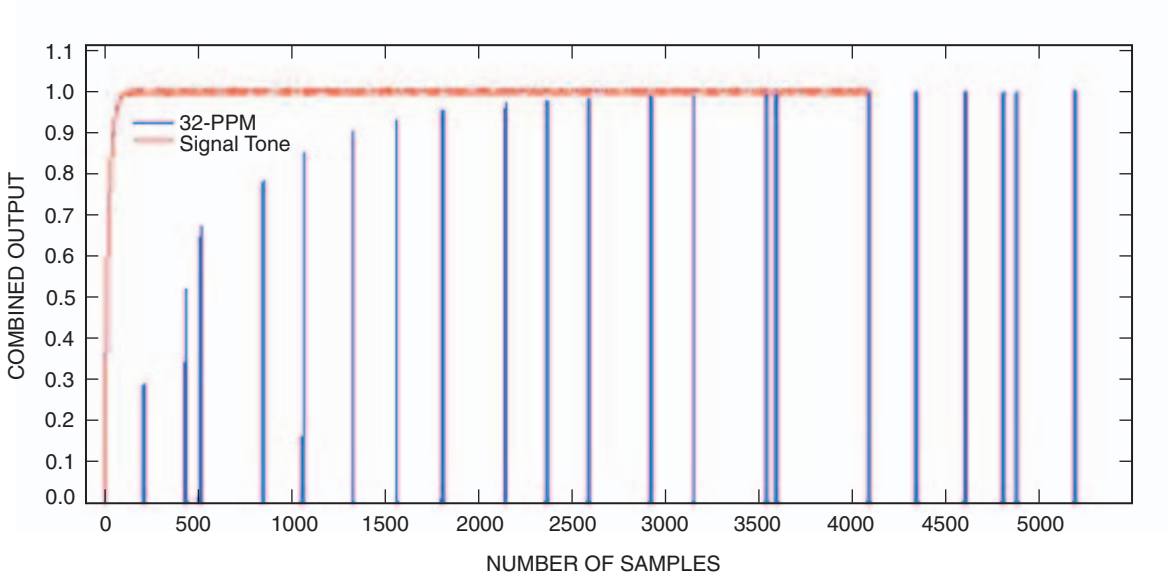

Fig. 16. Comparison of convergence for signal tone and 32-PPM signal.

1. Convergence of the LMS Algorithm with PPM Signals and No Atmospheric Turbulence. We first consider the case for a step size of $\mu = 1$ (considered to be small for the experimentally recorded data, which are on the order of 0.01 for the individual channels). The sum of the magnitudes of the signals in the four selected channels is approximately 0.186. Figure 17 shows the combined output (and weighted channel components) of the LMS combiner for this case. With a step size of 1, the LMS algorithm cannot keep up with the phase variations in the beat note. Hence, the combined output signal never reaches its maximum value of 0.186; instead, it reaches only about 0.037.

When a larger step size is used, $\mu = 7$, the combined output achieves the desired value of 0.186, as illustrated in Fig. 18. We see that the combined output reaches its desired maximum value after approximately 800 samples; this translates to an acquisition time of approximately 32 μs.

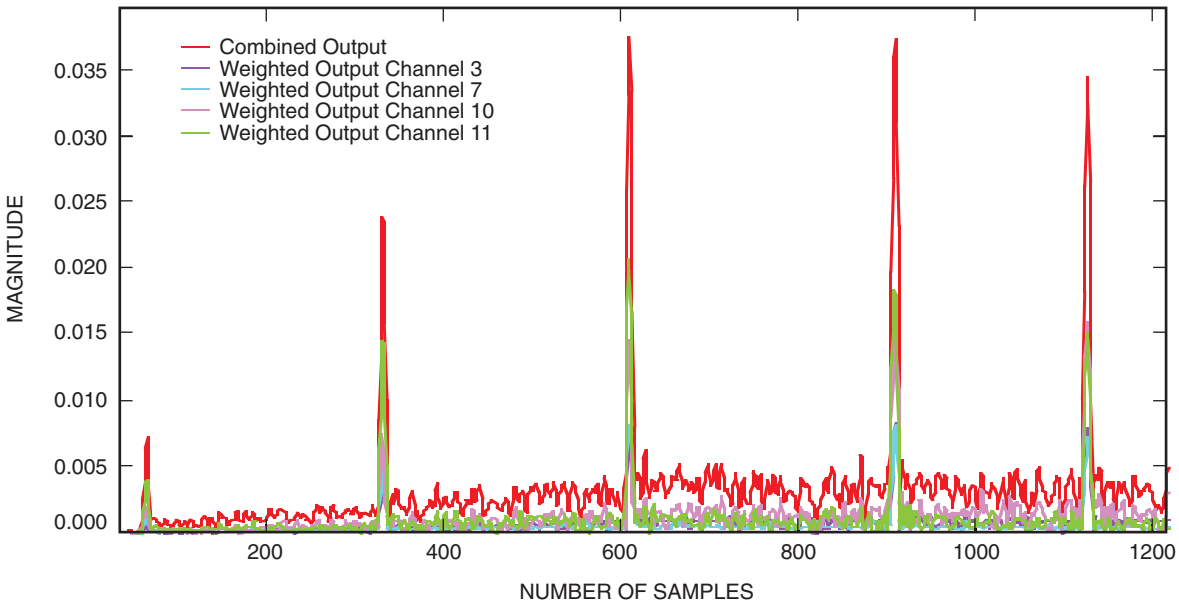

Fig. 17. Combined output with μ =1.

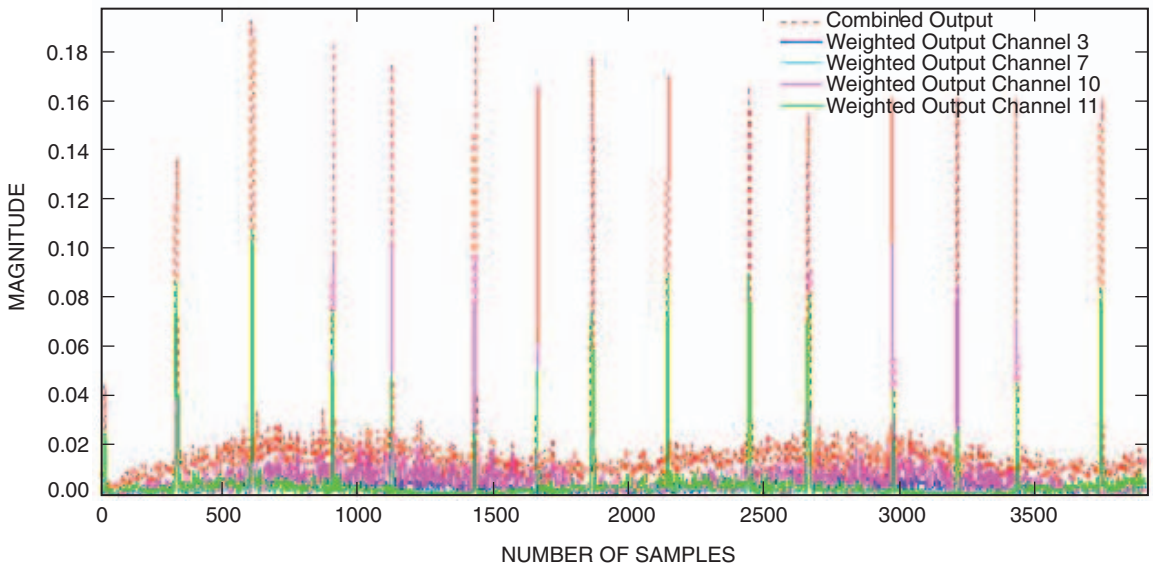

Fig. 18. Combined output with μ =7.

Figure 19 shows the behavior of the phase of the combining weights, as a function of time (or samples). We observe that the phase of the weights has a sawtooth shape due to the continuously changing phase in the downconverted output, which is not exactly at zero frequency.

Figure 20 also shows an individual combined pulse and its weighted components in greater detail. The addition of the magnitudes of the four channels is 0.186; indeed, the components sum to the expected value, verifying the validity of the instantaneous combining operation.

In summary, it can be seen that the experimentally obtained PPM signals are combined correctly with the larger step size, and they converge to their desired final value in less than a millisecond.

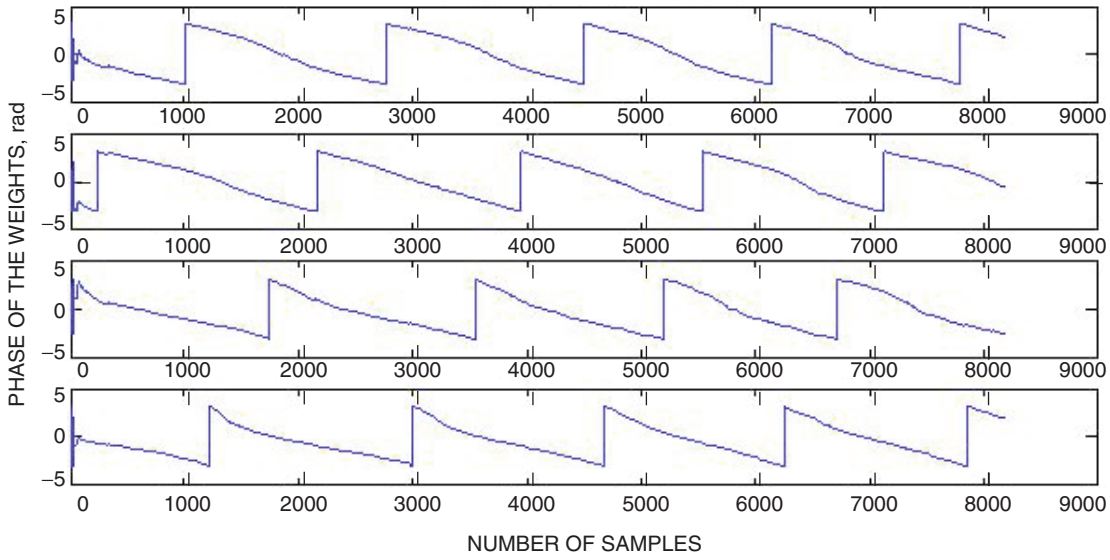

Fig. 19. Phase of the weights for $\mu = 7$ for four different channels.

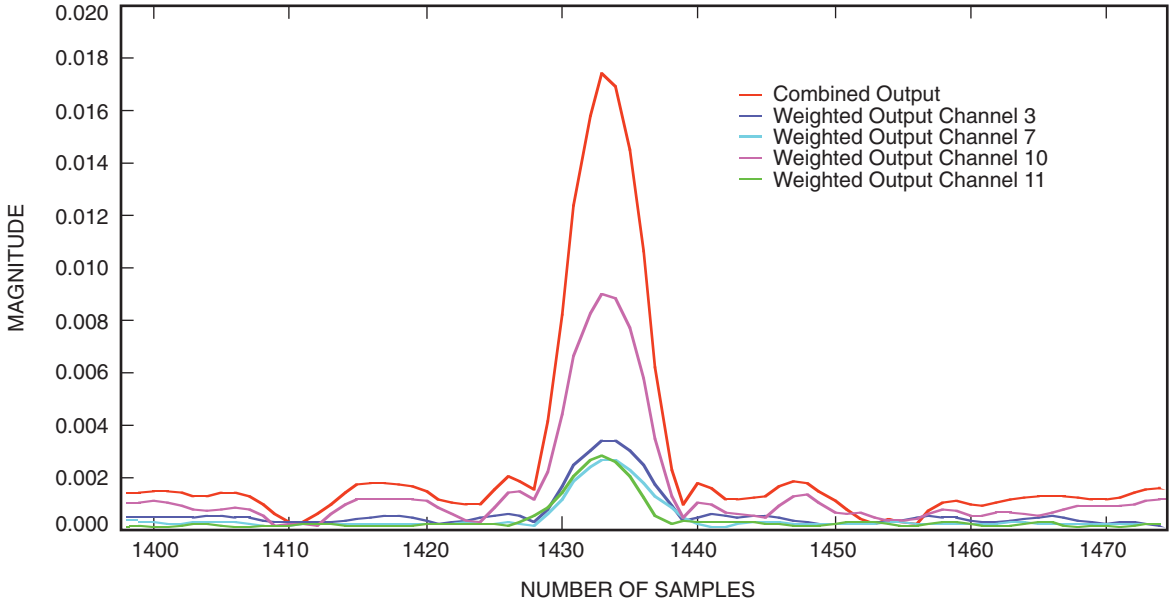

Fig. 20. Combined output and weighted signal components with $\mu = 7$.

2. Convergence of the LMS Algorithm in the Presence of Spatial Distortions Caused by a Static Plexiglass Plate in the Optical Path. For the case of combining detector array output signals spatially distorted by the plexiglass plate, the desired signal magnitude is the addition of the average magnitudes of the individual channels, which in this case turned out to be 0.063. Initially, we attempt to combine adaptively using a step size of 8; however, it can be seen from Fig. 21 that the step size is too small—hence, the LMS algorithm cannot keep up with the residual phase variations and only attains a magnitude of 0.033.

Referring to Figs. 22 through 24, we observe that, as we increase the value of the step size to $\mu = 22$, we get greatly improved combining performance. The combined output shown in Fig. 22 and in more detail

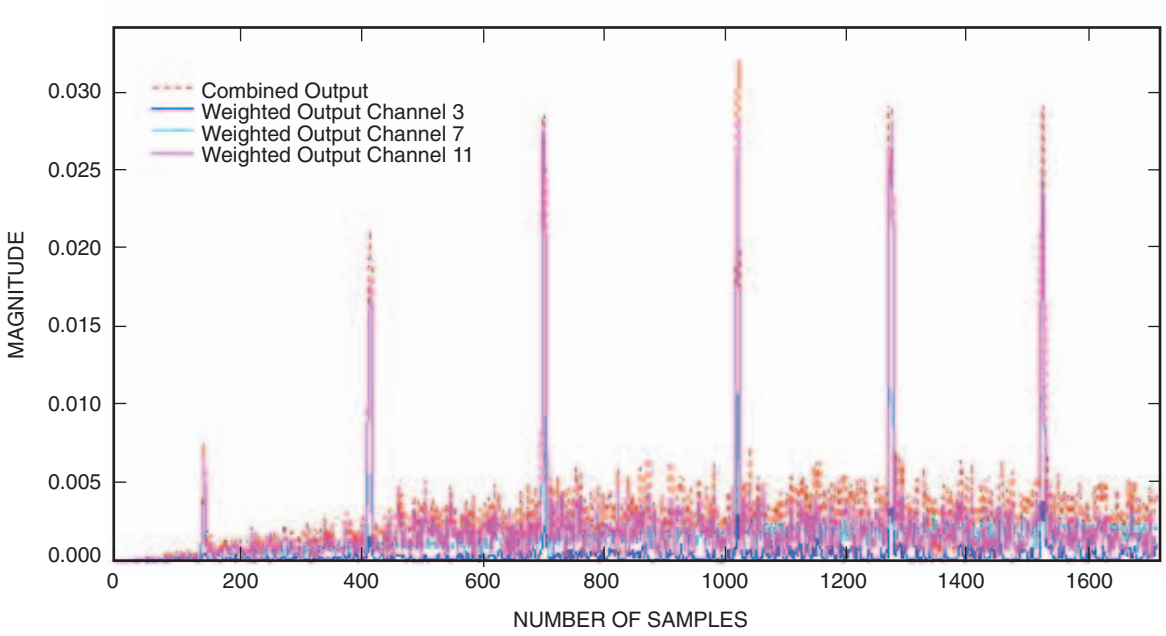

Fig. 21. Combined output with $\mu = 8$.

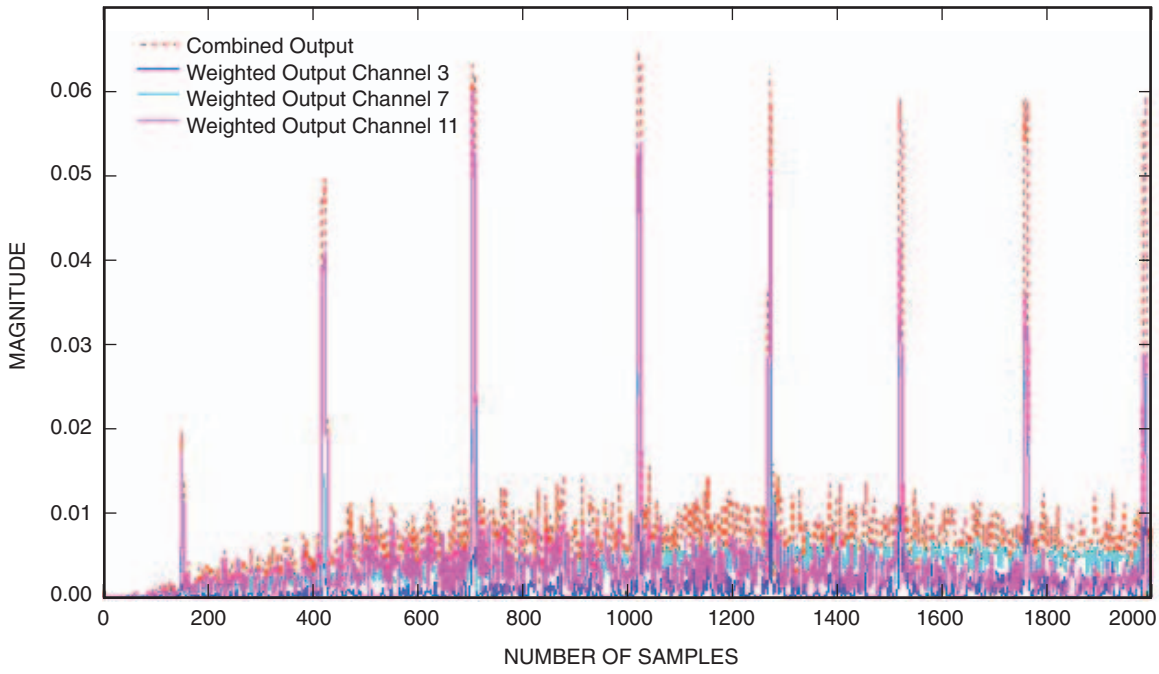

Fig. 22. Combined output with $\mu = 20$.

in Fig. 24 has increased, approaching its maximum value of 0.063. At this point, the step size is large enough that the LMS algorithm is able to keep up with the phase rotation of the complex downconverted beat note. These results illustrate that increasing the step size allows the LMS algorithm to follow and track the phase rotation of the complex downconverted beat note. For this value, there is accurate tracking of the signals and, accordingly, the error signal approaches zero, and maximum combined output is achieved.

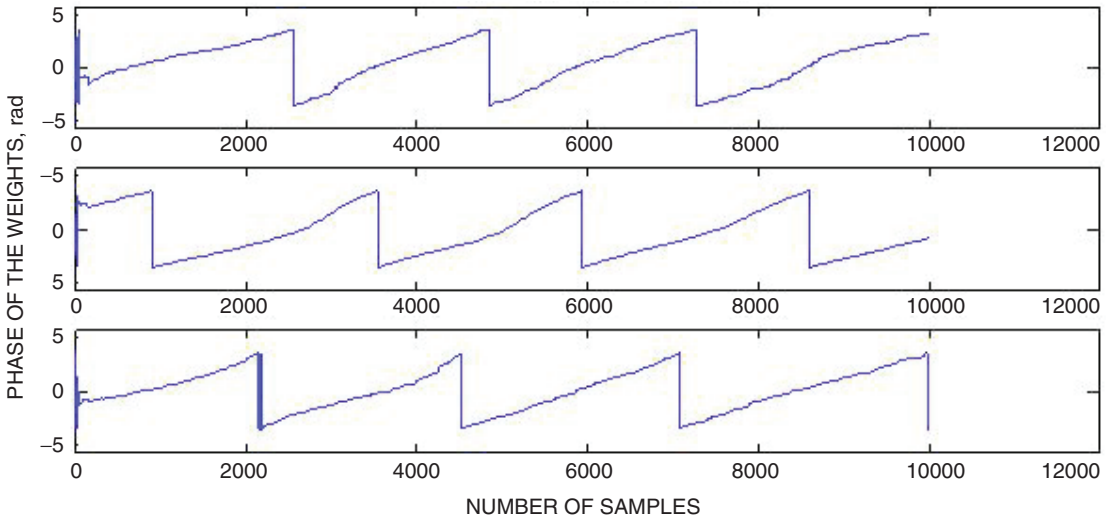

Fig. 23. Phase of the weights for $\mu = 22$ for four different channels.

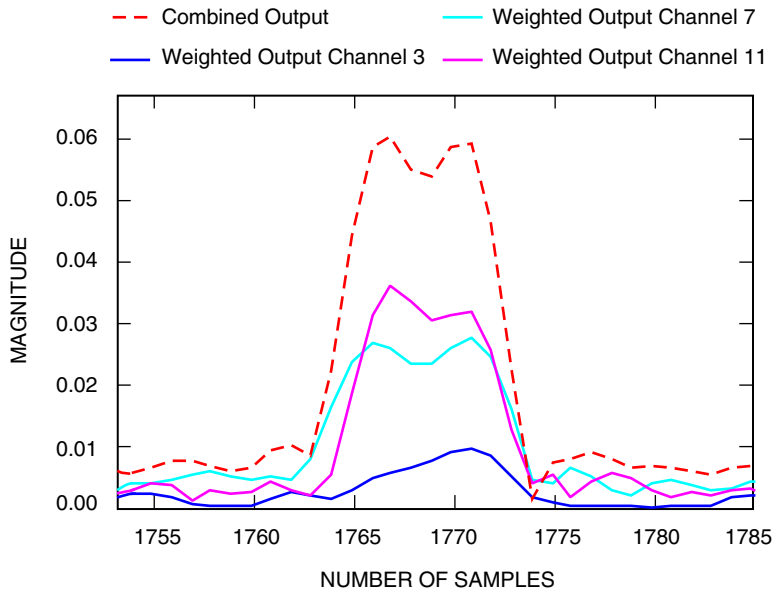

Fig. 24. Combined output with $\mu = 22$.

V. Conclusions and Future Work

Initial testing of an optical coherent communications receiver using PPM signals operating under simulated turbulence conditions has been completed. We have shown that a modified LMS algorithm can be used to track the phase of PPM signals generated by the photodetector array, producing an optimally combined signal. Work is continuing to detect the combined PPM signals and verify laboratory performance with theoretical results. Thus far, we have modulated the received optical field with PPM but maintained the pulse-to-pulse coherence of the optical fields, enabling the use of a simple modified version of the LMS algorithm. New algorithms are being developed for the case when the requirements for pulse-to-pulse coherence are relaxed; these algorithms, such as a suitably modified version of a constant modulus algorithm (CMA) and other appropriate algorithms for tracking pulsed laser signals received

under turbulent conditions, do not depend on temporal coherence on a short time scale. Finally, the experimental results of heterodyne-detected PPM will be related to theoretical optical homodyne PPM performance to demaonstrate shot-noise-limited operation.

Acknowledgments

The authors would like to acknowledge Carlos Esproles for his help on the laboratory setup and Angel Portillo for his simulations contributions.

References

[1] R. M. Gagliardi and S. Karp, *Optical Communications*, 2nd ed., Wiley Series in Telecommunications and Signal Processing, New York: John Wiley & Sons, Inc., 1995.

[2] M. Bass, ed., *Handbook of Optics, Fiber Optics and Nonlinear Optics*, 2nd ed., vol. IV, Chapter 1, New York: McGraw-Hill, 2001.

[3] J. C. Palais, *Fiber Optic Communications*, Chapter 10, New Jersey: Prentice Hall, 1998.

[4] G. R. Osche, *Optical Detection Theory for Laser Applications*, Chapter 1, Wiley Series in Pure and Applied Optics, New Jersey: John Wiley & Sons, Inc., 2002.

[5] A. Yariv, *Optical Electronics*, Chapter 11, Holt, Rinehart and Winston, Inc., 1985.

[6] S. B. Alexander, *Optical Communication Receiver Design*, Chapter 3, The Society of Photo-Optical Instrumentation Engineers, 1997.

[7] C. N. Georghiades and D. L. Snyder, "Receiver Performance for Heterodyne Optical Communication," *IEEE Transactions on Communications*, vol. Com-34, no. 11, November 1986.

[8] G. H. Einarsson, *Principles of Lightwave Communications*, Chapter 8, West Sussex, England: John Wiley & Sons, Ltd., 1996.

[9] J. M. Wozencraft and I. M. Jacobs, *Principles of Communication Engineering*, Chapter 4, New York: John Wiley & Sons, Inc., 1965.

[10] A. J. Viterbi, *Principles of Coherent Communications*, Chapter 8, New York: McGraw-Hill Book Company, 1966.

[11] B. Widrow and S. D. Stearns, *Adaptive Signal Processing*, Chapter 6, Prentice-Hall Signal Processing Series, New Jersey: Prentice-Hall Inc., 1985.

[12] R. T. Compton, Jr., *Adaptive Antennas*, Chapter 2, New Jersey: Prentice-Hall Inc., 1988.

Appendix

Derivation of Weight Values of the LMS Algorithm

For a desired signal $d(n) = 1$, and $\mu = 1$, and assuming that $\sum |S_i| = 1$, for $n = 1$ the following weights are obtained:

$$S_1 = \frac{1}{2}$$

$$S_2 = \frac{1}{2}e^{j\Delta_2}$$

$$W_1(1) = W_2(1) = 1$$

For $n = 1$:

$$y(1) = \frac{1}{2} + \frac{1}{2}e^{j\Delta_2}$$

$$e = \left(1 - \frac{1}{2} - \frac{1}{2}e^{j\Delta_2}\right) = \frac{1}{2} - \frac{1}{2}e^{j\Delta_2}$$

$$eS_2^* = \left(1 - \frac{1}{2} - \frac{1}{2}e^{j\Delta_2}\right)\frac{1}{2}e^{-j\Delta_2} = \frac{1}{4}\left(e^{-j\Delta_2} - 1\right)$$

$$eS_1^* = \left(\frac{1}{8} - \frac{1}{8}e^{j\Delta_2}\right)$$

with $\mu = 1$,

$$W_2(2) = 1 + \frac{1}{4}\left(e^{-j\Delta_2} - 1\right) = \frac{1}{4}\left(e^{-j\Delta_2} + 3\right)$$

$$W_1(2) = \frac{5}{4} - \frac{1}{4}e^{j\Delta_2}$$

For the cases of $n = 2$ and $n = 3$, the following analysis is shown:

For $n = 2$:

$$y(2) = \begin{pmatrix} \frac{1}{4}\left(5 - e^{j\Delta_2}\right) \\ \\ \frac{1}{4}\left(e^{-j\Delta_2} + 3\right) \end{pmatrix}^T \begin{pmatrix} \frac{1}{2} \\ \\ \frac{1}{2}e^{j\Delta_2} \end{pmatrix} = \frac{6}{8} + \frac{2}{8}e^{j\Delta_2}$$

$$e = 1 - y(2) = \frac{2}{8} - \frac{2}{8}e^{j\Delta_2}$$

$$eS_2^* = \left(\frac{2}{8} - \frac{2}{8}e^{j\Delta_2}\right)\frac{1}{2}e^{-j\Delta_2} = \frac{2}{16}e^{-j\Delta_2} - \frac{2}{16}$$

$$eS_1^* = \left(\frac{2}{16} - \frac{2}{16}e^{j\Delta_2}\right)$$

$$W_2(3) = \frac{6}{16}e^{-j\Delta_2} + \frac{10}{16}$$

$$W_1(3) = \frac{22}{16} - \frac{6}{16}e^{j\Delta_2}$$

For $n = 3$:

$$y(3) = \frac{28}{32} + \frac{4}{32}e^{j\Delta_2}$$

$$e(3) = 1 - y(3) = \frac{4}{32} - \frac{4}{32}e^{j\Delta_2}$$

$$eS_2^* = \frac{4}{64}e^{-j\Delta_2} - \frac{4}{64}$$

$$eS_1^* = \left(\frac{4}{64} - \frac{4}{64}e^{j\Delta_2}\right)$$

$$\omega_2(4) = \frac{36}{64} + \frac{28}{64}e^{-j\Delta_2}$$

$$\omega_1(4) = \frac{92}{64} + \frac{28}{64}e^{j\Delta_2}$$

These weight values were used to compute the output values of the LMS algorithm for the example shown in Fig. 14.